Estimation of stochastic behaviour in cardiac myocytes: I. Calcium movements inside the cytosol and sarcoplasmic reticulum on curvilinear domains

Serife Arif, Choi-Hong Lai, Nadarajah I Ramesh

Department of Mathematical Sciences, Faculty of Architecture, Computing and Humanities

University of Greenwich, London, UK

Abstract

Background: Since the discovery of Ca^{2+} sparks and their stochastic behaviour in cardiac myocytes, models have focused on the inclusion of stochasticity in their studies. While most models pay more attention to the stochastic modelling of cytosolic Ca^{2+} concentration the coupling of Ca^{2+} sparks and blinks in a stochastic model has not been explored fully. The cell morphology in past in silico studies is assumed to be Cartesian, spherical or cylindrical. The application on curvilinear grids can easily address this restriction and provide more realistic cell morphology. This paper presents a stochastic reaction-diffusion model that couples Ca^{2+} sparks and blinks applied to curvilinear domains.

Methodology: Transformation of the model was performed to the curvilinear coordinate system. A set of differential equations is used to produce Ca^{2+} waves initiated from sparks and blinks. A non-buffered and non-dyed version as well as a buffered and dyed version of these equations were studied in light of observing the effects of reactions on the Ca^{2+} wave properties. For comparison, results for both the Cartesian and curvilinear grids are provided.

Results and Conclusions: A successful demonstration of the application of curvilinear grids serving as basis for future developments.

Keywords

Stochastic calcium waves, Ca^{2+} sparks and blinks, curvilinear domain.

Introduction

Ca^{2+}-induced Ca^{2+} release (CICR) is the repeated process in which influx of extracellular Ca^{2+} into the cytosol from L-type channels triggers a release of Ca^{2+} from the sarcoplasmic reticulum (SR) through ryanodine receptors (RyRs) on the z-lines [1]. The CICR process is schematically illustrated in Figure 1 (a more detailed review of the processes leading to contraction can be found here [2]). The calcium release event appears as Ca^{2+} sparks [3, 4, 5, 6, 7, 8] in the cytosol and Ca^{2+} blinks [9] in the SR. The successive activation of RyRs increases the local Ca^{2+} concentration in the cytosol. This process is called calcium transient [10, 11, 12].

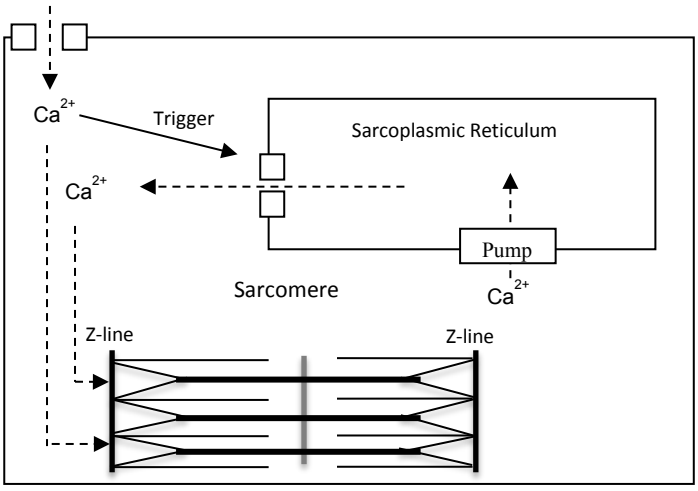

Figure 1. Schematic view of the influx and efflux of calcium in a cardiac myocyte. Ca^{2+} entry through L-type channels on the sarcolemma triggers Ca^{2+} release from the SR. This is a repeated process of the CICR mechanism. The calcium released from the SR increases the concentration in the cytosol. Ca^{2+} here travels to the sarcomeres and interacts with filaments and activates the contractile machinery. Upon relaxation, Ca^{2+} disassociates from the filaments and is pumped back into the SR by the SERCA pumps. Modified from [2].

It is of particular importance to understand the underlying mechanism of the CICR process since in cardiac ventricle cells spontaneous propagating waves of Ca^{2+} may occur due to Ca^{2+} overload which is believed to occur under pathological conditions. This can affect the heart's normal function and may lead to ventricular arrhythmias and heart failure [13, 14].

Ca^{2+} sparks in the heart muscle were first recorded by Cheng et al. (1993) [3]. Using confocal imaging and fluorescent indicator fluo-3, they observed discrete regions of increased fluorescence that varied in position between sequences of images that were taken 0.5 seconds apart. These increases correspond to spontaneous increases in intracellular Ca^{2+}, $[Ca^{2+}]_i$, known as Ca^{2+} sparks. The increases appear to originate from point sources of Ca^{2+} since they are restricted to circular regions. To investigate the origins of these sparks, cells were exposed to bathing medium without Ca^{2+} as to block entry of extracellular Ca^{2+} through sarcolemmal channels. This allowed them to investigate the role of SR Ca^{2+} release. Under normal physiological conditions it was found that the opening rate of the RyR was low and propagating CICR does not occur. The observed propagating waves of CICR was suggested to be due to the increased sensitivity of the CICR to the increase in $[Ca^{2+}]_i$.

Spatial non-uniformity was observed with the Ca^{2+} release [4] and it was found that these releases occur at discrete sites closely associated with transverse (t)-tubules at Z-lines [15] with regular spacing of 1.8-1.9μm longitudinally and more irregularly with a mean value of 0.79μm transversely [8]. There is no systematic spatial pattern in the spark occurrence and the occurrence varies temporally as well as spatially, therefore, exhibiting stochastic behaviour [4]. A study undertaken by Cannell et al. (1995) reported that the probability density function of the spark

occurrence fits a Poisson distribution, thus, supporting the idea that Ca^{2+} channel openings is a stochastic process [4].

Several models have been used to simulate the Ca^{2+} sparks and waves. A number of these models are partially based on the CICR process and the release from RyRs are described as either deterministic or stochastic. A non-exhaustive list of these models with a short description is given in Table 1 under two categories: deterministic and stochastic models. The models presented in Table 1 mainly consist of fractional differential equations (FDEs), partial differential equations (PDEs), and ordinary differential equations (ODEs).

Backx et al. (1989) described the CICR process with Magnesium buffer reactions using a one-dimensional model that only takes into account longitudinal diffusion [16]. The Ca^{2+} release from the SR occurs at calcium release units (CRUs) and is assumed to be a time dependent process with an exponential rise and fall of the Ca^{2+} flux from the SR. The occurrence was dependent on a threshold for Ca^{2+} concentration which lead to a deterministic description of this term in the model. A similar deterministic formulation was incorporated in the release flux by Soeller and Cannell (2002) which was then included in the total calcium current by volume integration [17]. The aim was to experimentally test the extraction of the release flux underlying calcium sparks including a more detailed dye and buffer binding structure.

Table 1. A non-exhaustive list of previously studied deterministic and stochastic models for the Ca^{2+} sparks and waves.

		FDE/PDE/ODE	Buffers and dye?	Citations
Deterministic	Backx et al. 1989	PDE, 6 ODEs	Yes	[16]
	Goldbeter et al. 1990	2 ODEs	No	[18]
	Dupont & Goldbeter, 1994; 1997	PDE, ODE	No	[19, 20]
	Smith et al. 1998	2 PDEs, 4 ODEs	Yes	[21]
	Izu et al. 1998, 2001a	2 PDEs, 2 ODEs	Yes	[22, 23]
	Soeller & Cannell, 2002	4 PDEs, 3 ODEs	Yes	[17]
	Tan et al. 2007	FDE, PDE, ODE	Yes	[24]
	Tracqui and Ohayon, 2009	PDE, ODE	No	[25]
	Li et al. 2011	2 FDEs, 4 ODEs	Yes	[26]
Stochastic	Izu et al. 2001b	2 PDEs, 2 ODEs	Yes	[27]
	Lu et al. 2010	2 PDEs, 2ODEs	Yes	[14]
	Chen et al. 2013, 2014	FDE, PDE, 4 ODEs	Yes	[28, 29]
	Li et al. 2017	FDE, 3 PDEs, 5 ODEs	Yes	[30]

Another deterministic construction of the SR calcium release was represented in 2 dimensional models [22, 23, 21] so the spatial and anisotropic properties of the cytosolic Ca^{2+} diffusion can

be successfully reproduced. In these models, the diffusion of Ca^{2+} sparks obeys Fick's Law. Later on, an anomalous subdiffusion model was proposed based on a FDE that represents the cytosolic Ca^{2+} concentration [24, 26] and it was shown to reproduce the spatial characteristic of sparks more realistically.

There has also been deterministic models with no buffer reactions included [18, 19, 20]. These models focused on representing the CICR process in a compartmental model with no dye and buffer reactions. No virtual point sources of CRUs are described. Instead the SR Ca^{2+} release is associated with a nonlinear term based on the cytosolic and sarcoplasmic concentrations applied to all spatial points of the computational domain. In 2009, this two-pool CICR model was integrated into a force-calcium relation by Tracqui and Ohayon to successfully reproduce Ca^{2+} waves and the resulting phases of contraction using cylindrical coordinates [25].

More recently, stochasticity is introduced into models [27] in which the Ca^{2+} channel opening depends on a probability function. The distribution of the CRUs were made discrete with longitudinal distancing of 2μm and transverse distancing of 0.4-0.8μm. Lu et al. (2010) integrated rogue RyRs into this model to simulate the effect of these receptors on the Ca^{2+} wave in ventricular myocytes with heart failure [14]. These models were extended from Fick's Law based Ca^{2+} diffusion to anomalous subdiffusion [28, 29]. Except for the work by Li et al. (2017) [30] the coupling of Ca^{2+} concentration in the cytosol to that in the SR has not been performed. Additionally, to this date models have been implemented on Cartesian, spherical [17] and cylindrical coordinates [31] which is a simplification towards representing the actual cell morphology. No stochastic or deterministic model are represented on curvilinear domains.

The aim of the present paper is the 1) extension of the stochastic formulation by Izu et al. (2001b) [27] to include the Ca^{2+} sparks coupled with Ca^{2+} blinks and its application on curvilinear domains (this allows one to work on real cell morphology); 2) representation of two different systems: a) buffered and dyed system to account for calcium movement observed in in vitro studies and b) non-buffered and non-dyed system to be able to distinguish the effects that reactions have on the dynamics; 3) comparison of the Cartesian and curvilinear domains. The model and its extension to curvilinear grids are described in the next section. The application to curvilinear grids and comparison results between models are presented in the results section with conclusions and potential future improvements discussed in the final section of this paper.

Methods

Mathematical model for Ca^{2+} sparks and Ca^{2+} blinks with buffer and dye

The set of differential equations (DEs) by Izu et al. (1998, 2001a, 2001b) [22, 23, 27] describing the cytosolic Ca^{2+} concentration with buffer and dye binding properties is modified to include an additional term for the cytosolic leak from [19, 20, 25] and a slightly different representation of the SR leak term [19, 20, 25]. An extension to this model here includes a coupling of the cytosolic Ca^{2+} diffusion with the sarcoplasmic Ca^{2+} concentration. For simplicity, diffusion is restricted to follow Fick's Law. Considering the above, the reaction-diffusion equations are expressed as

$$\frac{\partial C_{cyt}}{\partial t} = D_{Cx}\frac{\partial^2 C_{cyt}}{\partial x^2} + D_{Cy}\frac{\partial^2 C_{cyt}}{\partial y^2} + J_{dye} + J_{buffer} - J_{pump} - J_{Ca^{2+}\,leak} + J_{CRU} - J_{SR\,leak} \quad (1)$$

$$\frac{\partial C_{SR}}{\partial t} = J_{SR\ leak} + J_{pump} - J_{CRU} + J_{dye} + J_{buffer} \quad (2)$$

$$\frac{\partial [CaF]}{\partial t} = D_{Dx}\frac{\partial^2 [CaF]}{\partial x^2} + D_{Dy}\frac{\partial^2 [CaF]}{\partial y^2} - J_{dye} \quad (3)$$

$$\frac{\partial [CaB]}{\partial t} = -J_{buffer} \quad (4)$$

where $C_{cyt} = [Ca^{2+}]_{cyt}$ is the free Ca^{2+} concentration in the cytosol; $C_{SR} = [Ca^{2+}]_{SR}$ is the free Ca^{2+} concentration in the SR; $[CaF]$ and $[CaB]$ are the concentrations of Ca^{2+} bound dye and buffer; D_{Cx} and D_{Cy} are cytosolic Ca^{2+} diffusion coefficients in the longitudinal and transverse directions; D_{Dx} and D_{Dy} are diffusion coefficients of the Ca^{2+} bound dye in the longitudinal and transverse directions, respectively. Ca^{2+} diffusion is reported to be anisotropic [32] with diffusion twice as fast along the sarcomere orientation than that in the transverse direction [31]. Standard values used satisfy experimental data that $\frac{D_{Cy}}{D_{Cx}} = 0.5$ and are given in Table 2 along with a short description. Fluxes due to Ca^{2+} fluorescent indicator dye, J_{dye}, and endogenous stationary buffers, J_{buffer}, are

$$J_{dye} = -k_F^+ C_{cyt}([F]_T - [CaF]) + k_F^-[CaF]$$
$$J_{buffer} = -k_B^+ C_{cyt}([B]_T - [CaB]) + k_B^-[CaB]$$

k_j^+ and k_j^- are forward and reverse rate constants for dye ($j = F$) and buffer ($j = B$); $[F]_T$ and $[B]_T$ are total concentration of the indicator dye and buffers, values of which are given in Table 2. J_{pump}, $J_{Ca^{2+}\ leak}$, $J_{SR\ leak}$ represent the pumping rate of SR Ca^{2+}-ATPase, Ca^{2+} leak from the cytosol and SR, respectively. These are given as

$$J_{pump} = V_{pump}\frac{C_{cyt}^{npump}}{K_{pump}^{n_{pump}} + C_{cyt}^{n_{pump}}}$$
$$J_{Ca^{2+}\ leak} = kC_{cyt}$$
$$J_{SR\ leak} = k_f C_{SR}$$

in which V_{pump}, K_{pump} and n_{pump} represent the maximal rate, affinity constant and the Hill exponent for Ca^{2+} uptake into SR, while k and k_f are constants for Ca^{2+} efflux from cytosol to extracellular medium and from SR into cytosol, respectively.

Table 2. Standard parameter values [22, 23, 27, 28, 29].

Parameter	Value	Units	Notes
D_{Cx}, D_{Cy}	0.3, 0.15	$\mu m^2/ms$	Ca^{2+} diffusion coefficients
D_{Dx}, D_{Dy}	0.02, 0.01	$\mu m^2/ms$	Diffusion coefficients of dye
l_x, l_y	2, 0.8	μm	Spacing of CRUs in x and y
$[Ca^{2+}]_{cyt(\infty)}$	0.1	μM	Initial Ca^{2+} concentration
F	96500	$C\ mol^{-1}$	Faraday's constant
V_{pump}	0.208	$\mu M/ms$	Maximum SR pump rate

K_{pump}	0.184	μM	SR pump Michaelis constant
K_{prob}	15	μM	Ca^{2+} sensitivity parameter
n_{pump}, n_{prob}	3.9, 1.6	-	Hill coefficients
T_{open}	10	ms	Duration of current flow through CRU
P_{max}	0.3	per CRU ms^{-1}	Maximum probability of Ca^{2+} spark occurrence
σ_3	$I_{\mathrm{CRU}}/2F$	mole/ms	3 dimensional Ca^{2+} source strength
k_f^+, k_B^+	80, 100	$(\mu\mathrm{Ms})^{-1}$	Forward rate constants for dye and buffer reactions
k_f^-, k_B^-	90, 100	s^{-1}	Reverse rate constants for dye and buffer reactions
$[F]_T, [B]_T$	50, 123	μM	Total concentration (bound + unbound) of fluorescent dye and buffer

The SR Ca^{2+} release term, J_{CRU}, is expressed as [14, 27, 28, 29]

$$J_{CRU} = \sigma \sum_{i,j} \delta(x - x_i)\delta(y - y_j)S(x_i, y_j, t; T_{open}), \quad \sigma = K_s\sigma_3$$

Molar flux through the RyRs, σ, is associated with the source strength, K_S, and the 3 dimensional source strength, $\sigma_3 = I_{CRU}/2F$. K_s needs to be derived for a 2 dimensional model (See equation A1 in Appendix).

The CRUs are placed at regular intervals of l_x along the x-axis and l_y along the y-axis. It is assumed that once a CRU opens it will remain open for 10ms (i.e. $T_{open} = 10$) after which it will switch to a closed state and will not reopen (a long refractory period). An adjustment to the source strength was previously done to approximate the molar flux of a point source [23]. This approach is adopted here for a general 2 dimensional case [33] (See Appendix for the obtained σ values for the 2 dimensional case). The locations of the CRUs are identified through the Dirac delta function, δ where there is a channel (i.e. $x - x_i = 0$ implies that $\delta = 1$ which denotes there is a channel otherwise $x - x_i \neq 0$ indicates no channel $\delta = 0$). The stochastic term, S, controls the firing of the CRU when a probability condition is satisfied

$$S(x_i, y_j, t; T_{open}) = \begin{cases} 1, & P/P_{max} > u \\ 0, & P/P_{max} \leq u \end{cases}$$

where $P(C(x, y, t), K_{prob}, n_{prob}) = P_{max}C_{cyt}^{n_{prob}}/(K_{prob}^{n_{prob}} + C_{cyt}^{n_{prob}})$, P_{max} is the maximum probability of Ca^{2+} spark occurrence, K_{prob} represents the Ca^{2+} sensitivity factor and n_{prob} is the Hill coefficient. At each time step, Δt, a uniformly distributed random number, u, is generated and compared to the probability function P calculated from the Ca^{2+} concentration. A CRU fires if $P/P_{max} > u$ and thus $S = 1$ otherwise (i.e. in the case where $\frac{P}{P_{max}} < u$) a CRU will remain closed, i.e. $S = 0$.

Cartesian and curvilinear domains

Two different systems were solved on the Cartesian and curvilinear domains: 1) non-buffered and non-dyed (NBND) system (i.e. $J_{dye} = J_{buffer} = 0$) and; 2) buffered and dyed (BD) system.

Certain parameter values such as the initial SR Ca^{2+} concentration (i.e. $[Ca^{2+}]_{SR(\infty)}$), k, k_f, and I_{CRU} required modification when moving from a NBND system to a BD system in order to achieve a strong propagation of Ca^{2+} wave. These parameter values are given in Table 3.

Table 3. Parameter values for NBND and BD cases applied to the Cartesian and curvilinear grids. Some values used in the case of the BD system are within the range of the cited values.

	NBND		BD			
Parameter	Cartesian/Curvilinear	Source	Cartesian	Curvilinear	Source	Units
$[Ca^{2+}]_{SR(\infty)}$	750		1000	1000	[30]	μM
k	2	[25]	5	3	[19, 25]	s^{-1}
k_f	0.2	[25]	0.2	0.3	[19, 25]	s^{-1}
I_{CRU}	6		30	30		pA

A 2 dimensional domain is considered with the Cartesian and curvilinear grids shown in Figure 2. The Cartesian problem (Figure 2 - top) is solved with equations (1)-(4). Discretisation of the PDEs is performed using the alternating direction implicit (ADI) method. The ODE for the sarcoplasmic Ca^{2+} concentration is discretised using a 4th order Adams-Bashforth (AB) method and the other ODEs are discretised using the traditional forward Euler method.

In the curvilinear case, the diffusive equations (1) and (3) need to be transformed from the Cartesian based system to the curvilinear coordinate system prior to discretising. Transforming equations (1) and (3) they become

$$\frac{\partial C_{cyt}}{\partial t} = \left(D_{Cx}\left(\frac{\partial \xi}{\partial x}\right)^2 + D_{Cy}\left(\frac{\partial \xi}{\partial y}\right)^2\right)\frac{\partial^2 C_{cyt}}{\partial \xi^2} + 2\left(D_{Cx}\frac{\partial \xi}{\partial x}\frac{\partial \eta}{\partial x} + D_{Cy}\frac{\partial \xi}{\partial y}\frac{\partial \eta}{\partial y}\right)\frac{\partial^2 C_{cyt}}{\partial \xi \partial \eta} + \left(D_{Cx}\left(\frac{\partial \eta}{\partial x}\right)^2 + D_{Cy}\left(\frac{\partial \eta}{\partial y}\right)^2\right)\frac{\partial^2 C_{cyt}}{\partial \eta^2} + J_{dye} + J_{buffer} - J_{pump} - J_{Ca^{2+}\,leak} + J_{CRU} - J_{SR\,leak} \quad (5)$$

$$\frac{\partial [CaF]}{\partial t} = \left(D_{Dx}\left(\frac{\partial \xi}{\partial x}\right)^2 + D_{Dy}\left(\frac{\partial \xi}{\partial y}\right)^2\right)\frac{\partial^2 [CaF]}{\partial \xi^2} + 2\left(D_{Dx}\frac{\partial \xi}{\partial x}\frac{\partial \eta}{\partial x} + D_{Dy}\frac{\partial \xi}{\partial y}\frac{\partial \eta}{\partial y}\right)\frac{\partial^2 [CaF]}{\partial \xi \partial \eta} + \left(D_{Dx}\left(\frac{\partial \eta}{\partial x}\right)^2 + D_{Dy}\left(\frac{\partial \eta}{\partial y}\right)^2\right)\frac{\partial^2 [CaF]}{\partial \eta^2} - J_{dye} \quad (6)$$

These equations are then discretised using the ADI method. The source strength becomes spatially dependent since the distance between grid points will not be uniform. Equations (2), and (4)-(6) are then solved on the curvilinear grid (Figure 2 - bottom).

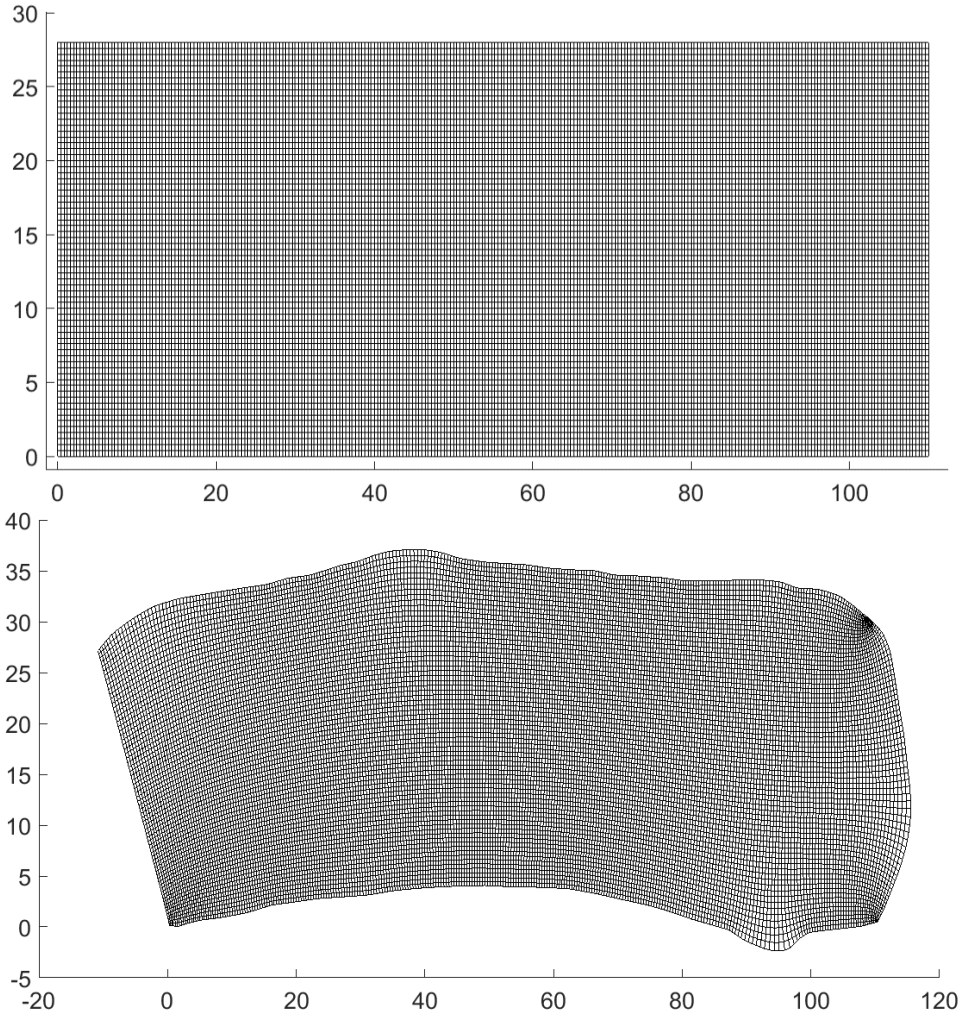

Figure 2. Grids generated on the Cartesian (top) and curvilinear (bottom) coordinate system. In both cases, the system is discretised into 276 x 71 grid points. A cell size of 110μm length and 28μm width is considered. Data for the generation of curvilinear coordinates is extracted from a successive snapshots of a real cell morphology provided by Tracqui and Ohayon (2009) at time t_4 [25]. The CRDT algorithm used in the generation of the curvilinear coordinates ensures the smooth distribution of the grid points throughout the curvilinear domain.

Orthogonal curvilinear coordinates are generated using the software gridgen-c developed by Sakov and CSIRO Marine Research (2000-2009) [See acknowledgement]. The code incorporates a CRDT algorithm by Driscoll and Vavasis (1998) for conformal mapping [34] which smoothly distributes the grid points throughout the domain.

The CRUs are distributed with $l_x = 2\mu$m spacing in the longitudinal and $l_y = 0.8\mu$m spacing in the transverse directions. In the curvilinear case, the number of spacing between CRUs is determined by setting equal number of grid points between channels leading to a pointwise evenly spread channels in both directions. The distribution of these channels are given on both Cartesian and curvilinear grids in Figure 3.

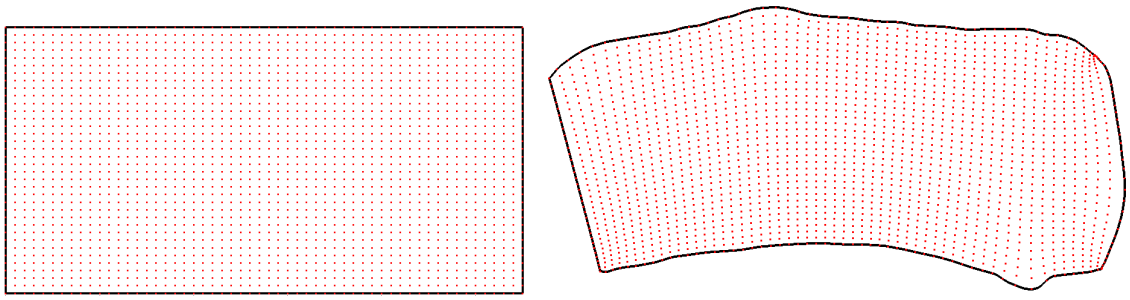

Figure 3. Distribution of the CRU channels on the Cartesian (left) and curvilinear (right) domains. The CRUs are uniformly distributed in the Cartesian case while in the curvilinear case, they are spaced out evenly with an equal number of grid points between them leading to the distribution to appear denser at the concave (top bending) and coarser at the convex (bottom bending) regions.

As boundary conditions zero-flux is assumed at the cell boundaries by imposing $\partial C_{cyt}/\partial x = \partial C_{cyt}/\partial y = 0$. Similar assumption is imposed on the equation for the Ca^{2+} bound dye, i.e. $\partial[CaF]/\partial x = \partial[CaF]/\partial y = 0$.

Results

In cardiac myocytes, Ca^{2+} waves propagate as sharp bands [35] with velocities and frequencies that are high enough to allow for the simultaneous propagation of distinct fronts in a given individual cell. The latter type of wave has been called type 1 for convenience [36].

In the following results, Ca^{2+} waves of type 1 is observed. Once sparks are initiated they develop in 10ms and increase the concentration around the region. The probability of firing is proportionally dependent on the local concentration. Therefore, a rise in concentration increases the probability of SR release and eventually leading to the activation of neighbouring CRUs. If the concentration is sufficiently high more CRUs fire consecutively which creates a propagating Ca^{2+} wave.

In all cases that are presented in this section, the initial cytosolic Ca^{2+} concentration at rest is set to $[Ca^{2+}]_{cyt(\infty)} = 0.1\mu$M. The concentration in the SR compartment is 500-1000 μM and is 2-3 orders of magnitude greater than that in the cytosol. Therefore, in the simulations presented here the initial concentration in the SR is set to 750 μM in the NBND system and 1000 μM in the BD systems. Simulations begin with 5x4 CRUs in the middle of the domain force activated in order to set off initial sparks. The temporal grids are set up with time step size of $\Delta t = 0.1$. The spatial step sizes in the Cartesian case are set to $\Delta x = \Delta y = 0.4$ and that in the curvilinear case is spatially dependent so will vary throughout the domain.

NBND system on the Cartesian and curvilinear domains

In this section, results are presented for the NBND system. The set of equations (1)-(4) are solved on the Cartesian domain and equations (2) and (4)-(6) on the curvilinear domain. Buffer and dye reactions are neglected in the model, i.e. $J_{dye} = J_{buffer} = 0$, in order to observe the

effects of such reactions on the wave propagation velocity and amplitude. Solving the NBND system on both the Cartesian and curvilinear domains with the CRU distribution given in Figure 3, we obtain the results in Figures 4 (Cartesian) and 5 (curvilinear). Images show the development of the initial sparks in 10ms and its propagation towards and along the boundaries at the top and bottom until it reaches and propagates outwards from the boundaries at the ends (left and right).

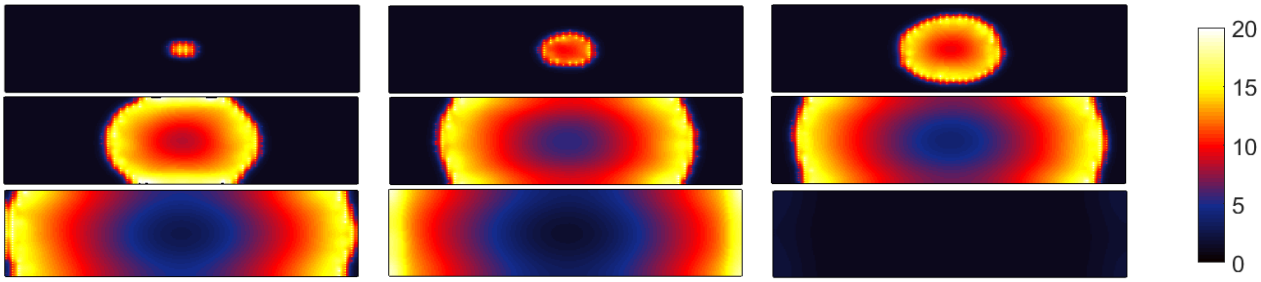

Figure 4. Ca^{2+} wave propagation on the Cartesian grid in the absence of buffer and dye reactions. Snapshots are recorded at times 10, 25, 50, 75, 125, 150, 175, 190 and 300 ms (left to right, top to bottom). The colourbar denotes the Ca^{2+} concentration in μM.

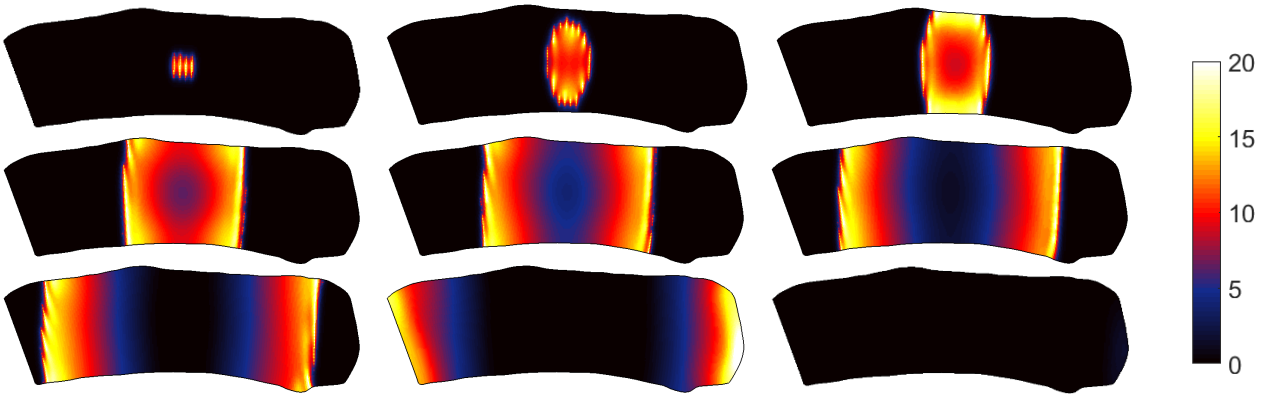

Figure 5. Ca^{2+} wave propagation on the curvilinear grid in the absence of buffer and dye reactions. Snapshots are recorded at times 10, 40, 70, 125, 175, 225, 275, 375 and 550 ms (left to right, top to bottom). The colourbar denotes the Ca^{2+} concentration in μM.

Looking at the simulation time when the Ca^{2+} reaches the end boundaries it was observed that the wave propagates in less time compared to that in the curvilinear case. As can be seen in Figure 6, the peak of the wave exits the domain in 200ms in the Cartesian (Figure 6 - a) and 400ms in the curvilinear (Figure 6 - b) cases. The longitudinal velocity of the wave is calculated to be approximately $289\mu m/s$ with amplitudes approximately ranging 17.1-19.3μM in the Cartesian (Figure 7 - a) and $153\mu m/s$ with amplitudes approximately ranging 19.2-23.3μM in the curvilinear cases (Figure 7 - c).

There is a periodic exchange of Ca^{2+} between the SR and the cytosol. These result in the mentioned Ca^{2+} sparks and blinks, the simulation results of which are presented in Figure 7. There is a slight difference in the amplitude of the cytosolic concentration profiles when comparing the Cartesian and curvilinear problems. Similarly, there is not much variation in the sarcoplasmic concentration profiles when comparing the solution on the two different domains.

In the Cartesian case, concentration in the SR drops to approximately 581μM while this drop in the curvilinear case is approximately between 576μM and 586μM (See Figure 7 – b and d).

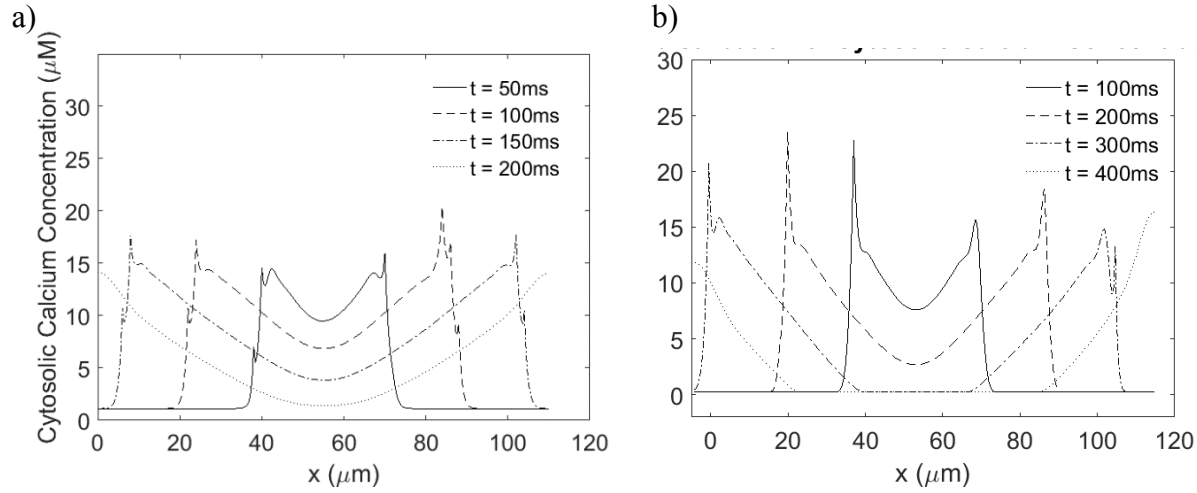

Figure 6. Cytosolic Ca^{2+} wave propagation without buffer and dye reactions. The spatial characteristics of the wave propagation are plotted on the (a) Cartesian domain at times 50, 100, 150 and 200 ms and (b) curvilinear domain at times 100, 200, 300 and 400ms.

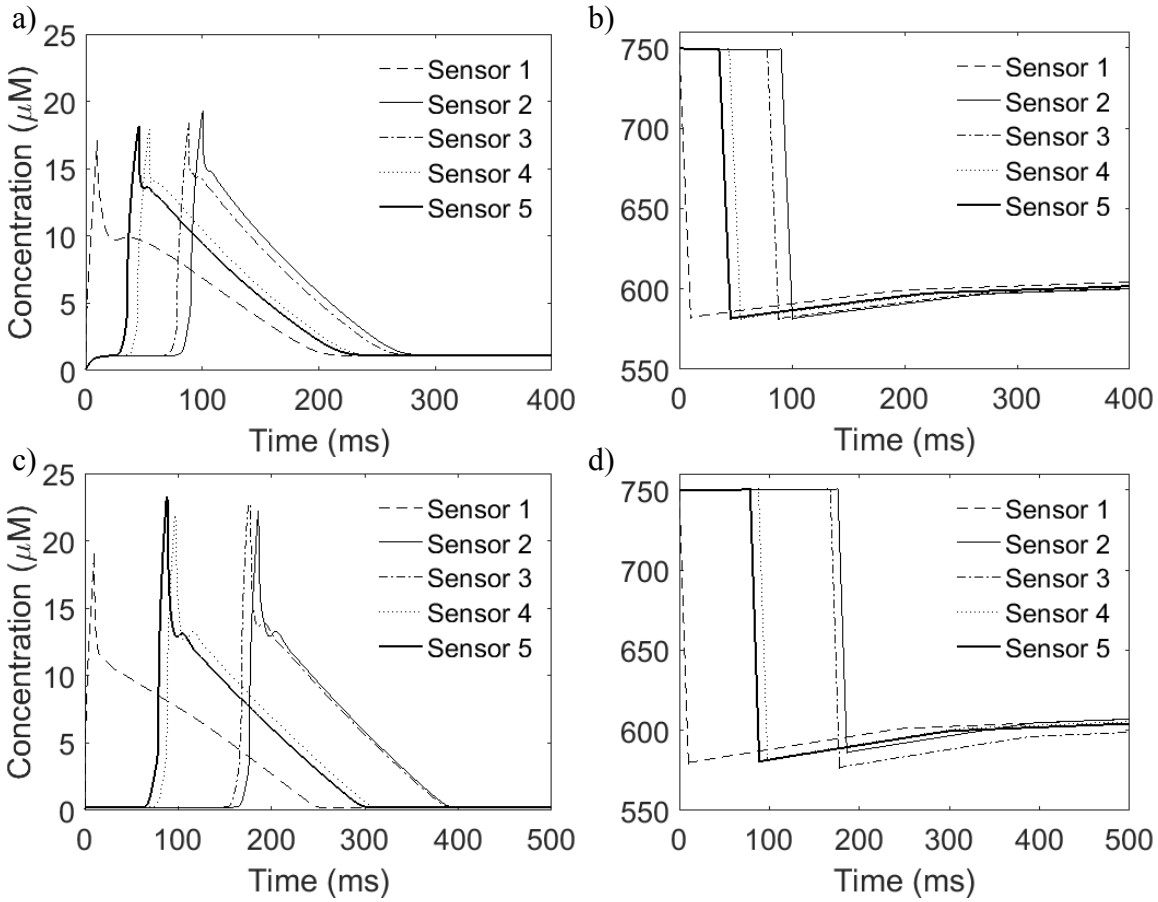

Figure 7. Cytosolic (a and c) and sarcoplasmic (b and d) Ca^{2+} concentrations are plotted on the Cartesian (a and b) and curvilinear (c and d) domains. Sensor 1 corresponds to a channel at the centre of the cell. Sensors 4 and 5 are 10μm away from sensor 1 on either side in the x-direction. Sensors 2 and 3 are quarter of the way in from the left and right edges, respectively.

BD system on the Cartesian and curvilinear domains

In this section, results are presented for the BD system. The same set of equations as in the previous section are solved but with reactions included, i.e. $J_{dye} \neq 0, J_{buffer} \neq 0$. Figures 8 and 9 show the Ca^{2+} wave propagation in the presence of buffer and dye reactions. The wave velocity is observed to be approximately 113-114μm/s in the Cartesian and 111μm/s in the curvilinear coordinates. Figure 10 shows the time course of the Ca^{2+} wave at times $t = 100, 200, 300$ and 400ms (a and c) and the normalised fluorescent indicator dye profile, F/F_0 (b and d). The normalised fluorescent indicator profile is recorded at the cell centre.

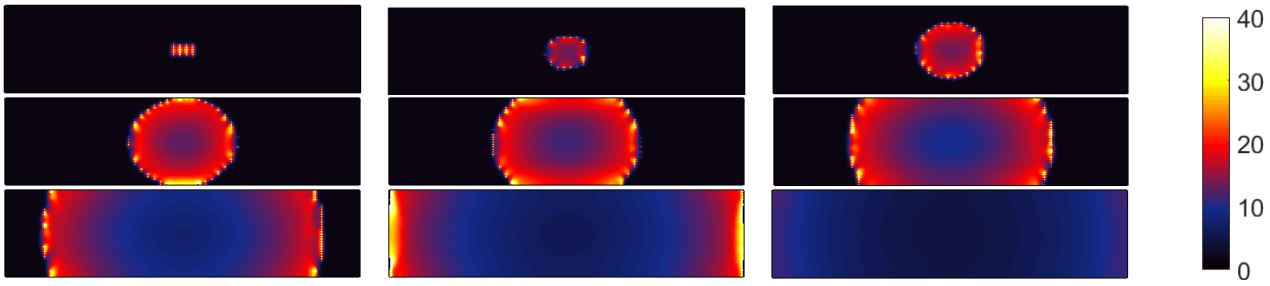

Figure 8. Ca^{2+} wave propagation on the Cartesian grid in the presence of buffer and dye reactions. Snapshots are recorded at times 10, 40, 75, 125, 175, 250, 350, 460 and 600 ms (left to right, top to bottom). The colourbar denotes the Ca^{2+} concentration in μM.

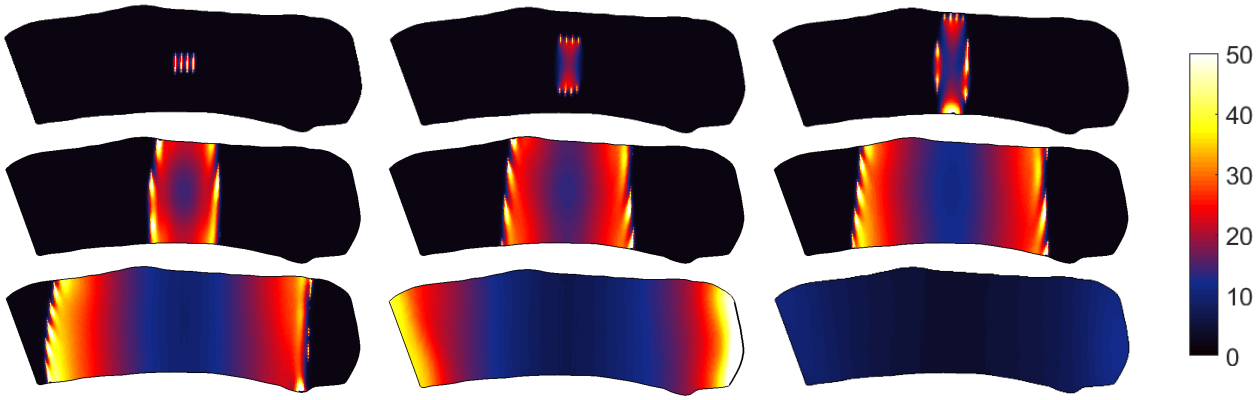

Figure 9. Ca^{2+} wave propagation on the curvilinear grid in the presence of buffer and dye reactions. Snapshots are recorded at times 10, 40, 75, 150, 250, 350, 450, 600 and 900 ms (top to bottom left to right). The colourbar denotes the Ca^{2+} concentration in μM.

The Ca^{2+} concentration increases rapidly initially thus a steep rise in the normalised fluorescent value. The concentration is high enough so that neighbouring sites will activate eventually leading to wave of Ca^{2+}. As Ca^{2+} propagates from the region the concentration will decrease leading to a decrease in the normalised fluorescent values. F/F_0 profile peaks at 1.129 and 1.135 in the Cartesian and curvilinear cases, respectively. The shape observed around the peak and the pattern of rise and fall is also observed in experimental [3-6, 8, 9, 17, 37- 39] and other numerical studies [17, 21, 24, 26].

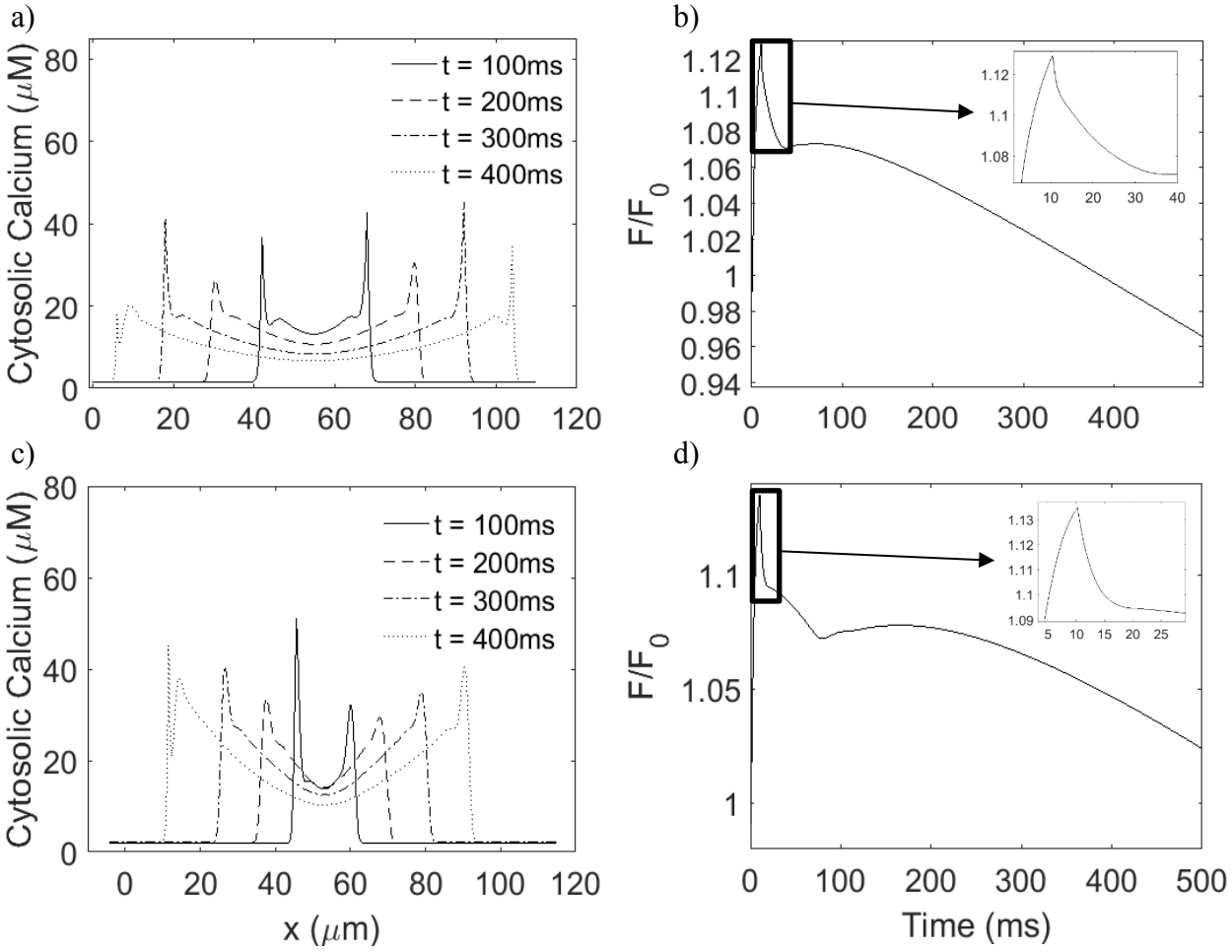

Figure 10. Ca^{2+} wave propagation without buffer and dye reactions. The spatial characteristics of the wave propagation are plotted at times 100, 200, 300 and 400 ms on the (a) Cartesian and (c) curvilinear domains.

A large variation is observed in the sparks and blinks (Figure 11). The amplitude of the sparks range 41.3-47.5μM with 81.7-85.2μM drop in SR Ca^{2+} content in the Cartesian case (Figure 11 - a) and that in the curvilinear case are 56.7-79μM for spark amplitude and 14.6-58.1μM for drop in SR Ca^{2+} concentration (Figure 11 - c).

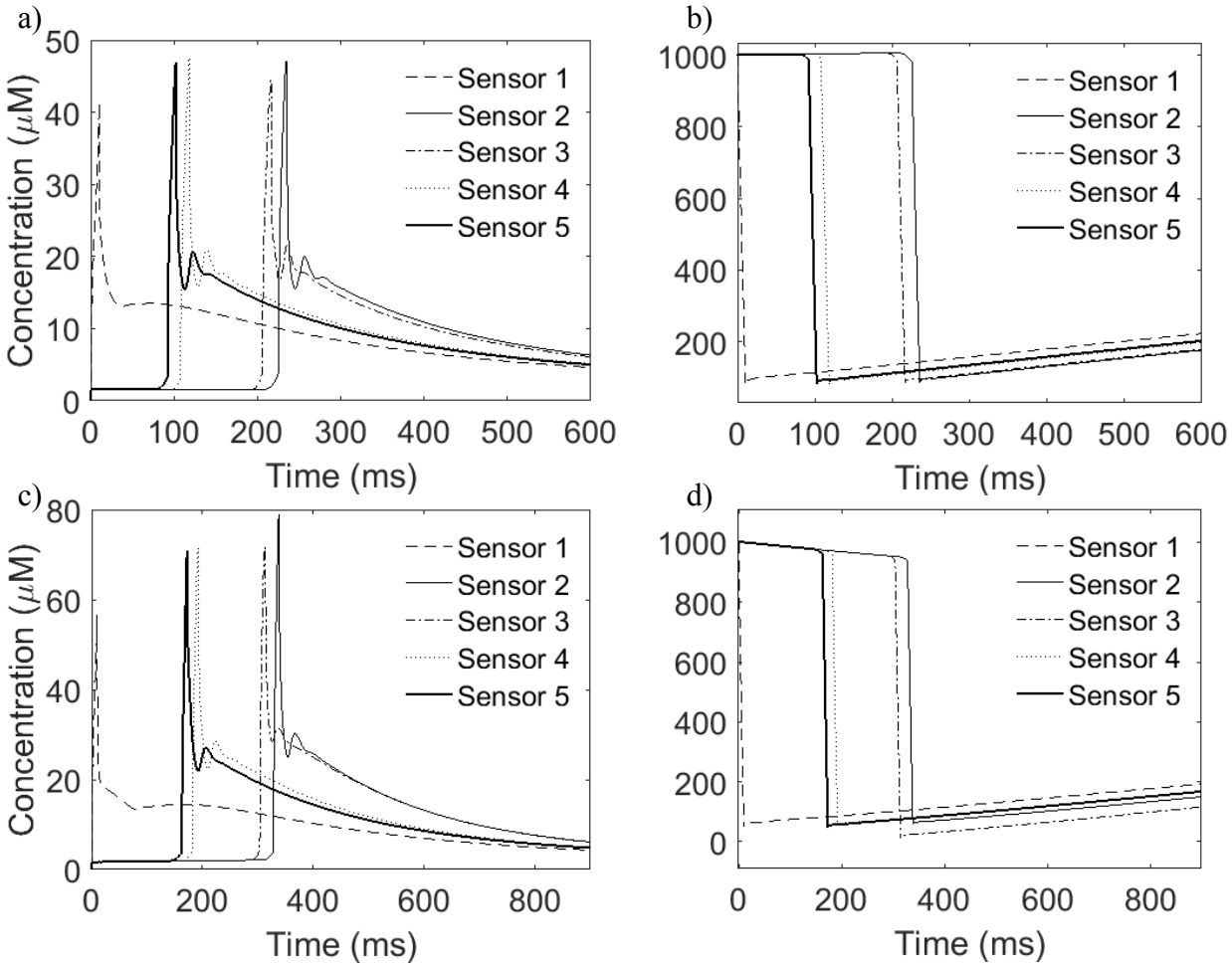

Figure 11. Time course of the Ca^{2+} wave propagation located at sensors 1-5. Cytosolic Ca^{2+} concentrations are plotted on the (a) Cartesian and (c) curvilinear domains. Similarly, sarcoplasmic Ca^{2+} concentrations are plotted on the (b) Cartesian and (d) curvilinear domains. Sensor 1 corresponds to a channel at the centre of the cell. Sensors 4 and 5 are 10μm away from sensor 1 towards either side. Sensors 2 and 3 are quarter way in from the left and right edges, respectively.

Discussion and conclusion

In this paper, the application of Ca^{2+} waves on the curvilinear grids is successfully demonstrated with comparisons against the Cartesian case. This enables the quantitative analysis on Ca^{2+} sparks/blinks and waves by taking into account more realistic cell morphology. The in silico study undertaken here included BD and NBND systems to distinguish the effects of reactions on the Ca^{2+} wave propagation on the Cartesian and curvilinear grids separately. It has been shown that in the case of the NBND system although not much variation was observed in the amplitudes of the cytosolic and sarcoplasmic Ca^{2+} concentration profiles, the wave velocity in the Cartesian case was much higher (almost twice as much) than that in the curvilinear case (which is closer to the experimentally observed value of 100μm/s). Adding buffer and dye to the system has dramatically changed the velocity and amplitude of the wave. Decrease in velocity was observed. The cytosolic Ca^{2+} amplitudes have increased by approximately 2.4 fold and SR Ca^{2+} content

drops to as much as approximately 6.85-7.1 fold in the Cartesian case whilst in the curvilinear case cytosolic Ca^{2+} have increased by roughly 3.5 times with a drop in SR Ca^{2+} content by 10-39 fold. In both the BD and NBND cases the wave velocity calculated on the curvilinear coordinate system provided a closer estimate to that observed experimentally (i.e. 100μm/s). In the BD cases, the fluorescent indicator dye profiles follow a pattern which is recorded experimentally.

The formation and development of Ca^{2+} sparks into waves appear differently in the Cartesian and curvilinear grids. The wave propagation region appears to be more elongated in the y-direction for the curvilinear cases. This may be due to either the distribution of CRUs being grid dependent or the partially contracted state of the cell morphology making the bottom half of the CRUs more dense and the top half coarser compared to the central part of the cell. The underlying algorithms used in the generation of curvilinear grid points ensure the orthogonal and conformal mapping of the grid points. Therefore, some regions will be densely or coarsely populated with grid points. Therefore, the distribution of CRUs will be dense or coarse in the respective regions accordingly. Having a spatially dependent distribution rather than a grid dependent one will make the curvilinear model more realistic since it is known that CRUs are longitudinally 2μm and transversely 0.4-0.8μm apart.

A single ODE was used as an update for a general buffer term. However, it is known that Ca^{2+} can bind to buffers consisting of calmodulin, troponin C, binding sites on the SR and sarcolemmal (SL) membranes. Therefore, a more detailed model must be incorporated to account for these buffers separately. Additionally, Ca^{2+} bound buffers and dye in the SR has different reaction and diffusional properties than that in the cytosol. Therefore, an additional set of equations accounting for this would make this model more comparable to the real case scenario. For the sarcoplasmic Ca^{2+} concentration, an ODE has been used. However, diffusion is also present in this compartment so a PDE can be used to account for this.

Recently, it has been shown that cytosolic Ca^{2+} diffusion follows an anomalous subdiffusion rather than Fick's Law. Fick's Law is known to produce Ca^{2+} full-width at half maximum (FWHM) of 1μm, half of which is observed experimentally. Anomalous subdiffusion is known to get around this issue and produce FWHM of closer to 2μm. Here transformation to curvilinear coordinates is more straightforward with Fick's Law based diffusion. Bearing this in mind this simplification was maintained in order to demonstrate the application. The model presented in this paper can always be extended to an anomalous subdiffusion model.

Appendix

The numerical conversion for the source strength, K_s, involves the Green's function obtained from the analytical solution of the diffusion problem for the 2 dimensional case and convolving this with the Heaviside function. Some description on the derivation is given previously [27]. The deduced relations for each of the Cartesian and curvilinear cases are given below. For an anisotropic case where $D_{Cx} = 0.3\mu\text{m}^2/\text{ms}$ and $D_{Cy} = D_{Cz} = 0.15\mu\text{m}^2/\text{ms}$ the following is obtained for the molar flux, σ, that contains the source strength

$$\sigma = \frac{7.74596669\left(1 - \text{erf}\left(0.05270462768\sqrt{30\left(\Delta x^2 + 2(\Delta y^2 + \Delta z^2)\right)}\right)\right)}{\sqrt{30\left(x^2 + 2(y^2 + z^2)\right)E_1(0.08333333333\Delta x^2 + 0.1666666667\Delta y^2)}}\sigma_3 \qquad \text{A.1}$$

where $E_1(x) = \int_z^\infty \frac{e^{-t}}{t} dt$ is an exponential integral. $\Delta x, \Delta y$ and Δz are distances between points in the x, y and z directions, respectively. In the case of the Cartesian coordinates, the molar flux is a scalar. However, in curvilinear coordinates, it is spatially dependent and becomes a vector.

Acknowledgements
The authors are greatly thankful to fellow researcher, Christopher Beckwith, for his assistance on generating the orthogonal curvilinear grids. The authors would also like to acknowledge the orthogonal grid generator (gridgen-c) provided by Pavel Sakov and CSIRO Marine Research (2006-2017). The code gridgen-c is available at https://github.com/sakov/gridgen-c.

Declaration of conflicting interests
The authors declare that there is no conflict of interest.

Funding
The authors disclosed receipt of the following financial support for the research, authorship, and publication of this article: This work was supported by a Vice-Chancellor's PhD scholarship of the University of Greenwich (Reference Number: VCS-ACH-15-14).

Contributorship
All authors contributed equally to the study conception, methodology implementation and manuscript drafting.

References

[1] Fabiato A. Calcium-induced release of calcium from the cardiac sarcoplasmic reticulum. *Am J Physiol* 1983; 245: C1-C14.

[2] Arif S, Natkunam K, Buyandelger B, et al. An inverse problem approach to identify the internal force of a mechanosensation process in a cardiac myocyte. *Inform Med Unlocked* 2017a; 6: 36-42.

[3] Cheng H, Lederer WJ and Cannell MB. Calcium sparks: elementary events underlying excitation-contraction coupling in heart muscle. *Science* 1993; 262: 740-744.

[4] Cannell MB, Cheng H and Lederer WJ. The control of calcium release in heart muscle. *Science* 1995; 268: 1045-1049.

[5] Cheng H, Lederer MR, Lederer WJ, et al. Calcium sparks and [Ca2+]i waves in cardiac myocytes. *Am J Physiol* 1996a; 270: C148-C159.

[6] Cheng H, Lederer MR, Xiao R-P, et al. Excitation-contraction coupling in heart: new insights from Ca2+ sparks. *Cell Calcium* 1996b; 20: 129-140.

[7] Santana LF, Cheng H, Gomez AM, et al. Relation between the sarcolemmal Ca2+ current and Ca2+ sparks and local control theories for cardiac excitation-contraction coupling. *Circ Res* 1996; 78: 166-171.

[8] Parker I, Zang W-J, and Wier WG. Ca2+ sparks involving multiple Ca2+ release sites along Z-lines in rat heart cells. *J Physiol* 1996; 497: 31-38.

[9] Brochet DXP, Yang D, Maio AD, et al. Ca2+ blinks: Rapid nanoscopic store calcium signalling. *PNAS* 2005; 102: 3099-3104.

[10] Fabiato A. Simulated calcium current can both cause calcium loading in and trigger calcium release from the sarcoplasmic reticulum of a skinned canine cardiac Purkinje cell. *J Gen Physiol* 1985b; 85:291-320.

[11] Fabiato A. Time and calcium dependence of activation and inactivation of calcium-induced release of calcium from the sarcoplasmic reticulum of a skinned canine cardiac purkinje cell. *J Gen Physiol* 1985d; 85: 247-289.

[12] Lopez-Lopez JR, Shacklock PS, Balke CW, et al. Local calcium transients triggered by single l-type calcium channel currents in cardiac cells. *Science* 1995; 268: 1042-1045.

[13] Lakatta EG and Guarnieri T. Spontaneous myocardial calcium oscillations: are they linked to ventricular fibrillation. *J Cardiovasc Electrophysiol* 1992; 44: 73-89.

[14] Lu L, Xia L, Ye X, et al. Simulation of the effect of rogue ryanodine receptors on a calcium wave in ventricular myocytes with heart failure. *Phys Biol* 2010; 7: 026005.

[15] Shacklock PS, Wier WG, Balke CW. Local Ca^{2+} transients (Ca^{2+} sparks) originate at the transverse tubules in rat heart cells. *J Physiol (Lond)* 1995; 487: 601-608.

[16] Backx PH, Tombe PPD, Deen JHKV, et al. A model of propagating calcium-induced calcium release mediated by calcium diffusion. *J Gen Physiol* 1989; 93: 963-977.

[17] Soeller C, Cannell MB. Estimation of the sarcoplasmic reticulum Ca2+ release flux underlying Ca2+ sparks. *Biophys J* 2002; 82: 2396-2414.

[18] Goldbeter A, Dupont G, Berridge MJ. Minimal model for signal-induced Ca^{2+} oscillations and for their frequency encoding through protein phosphorylation. *Proc Natl Acad Sci USA* 1990; 87: 1461-1465.

[19] Dupont G, Goldbeter A. Properties of intracellular Ca2+ waves generated by a model based on Ca2+-induced Ca2+ release. *Biophys J* 1994; 67: 2191-2204.

[20] Dupont G, Goldbeter A. Modelling oscillating and waves of cytosolic calcium. *Nonlinear Anal Theory Meth Appl* 1997; 30: 1781-1792.

[21] Smith GD, Keizer JE, Stern MD, et al. A simple numerical model of calcium spark formation and detection in cardiac myocytes. *Biophys J* 1998; 75: 15-32.

[22] Izu LT, Wier WG, Balke CW. Theoretical analysis of the Ca2+ spark amplitude distribution. *Biophys J* 1998; 75: 1144-1162.

[23] Izu LT, Mauban JRH, Balke CW, et al. Large currents generate cardiac Ca2+ sparks. *Biophys J* 2001a; 80: 88-102.

[24] Tan W, Fu C, Xie W, et al. An anomalous subdiffusion model for calcium spark in cardiac myocytes. *Appl Phys Lett* 2007; 91: 183901.

[25] Tracqui P, Ohayon J. An integrated formulation of anisotropic force-calcium relations driving spatio-temporal contractions of cardiac myocytes. *Phil Trans R Soc A* 2009; 367: 4887-4905.

[26] Li K, Fu C, Cheng H, et al. Anomalous subdiffusion of calcium spark in cardiac myocytes. *Cell Mol Bioeng* 2011; 4: 457-465.

[27] Izu LT, Wier WG, and Balke CW. Evolution of cardiac calcium waves from stochastic calcium sparks. *Biophys J* 2001b; 80: 103-120.

[28] Chen X, Kang J, Fu C, et al. Modelling calcium wave based on anomalous subdiffusion of calcium sparks in cardiac myocytes. *PLoS ONE* 2013; 8: e57093.

[29] Chen X, Guo L, Kang J, et al. Calcium waves initiating from the anomalous subdiffusive calcium sparks. *J R Soc* 2014; 11: 20130934.

[30] Li J, Xie W, Chen X, et al. A novel stochastic reaction-diffusion model of Ca^{2+} blink in cardiac myocytes. *Science Bulletin* 2017; 62: 5-8.

[31] Subramanian S, Viatchenko-Karpinski S, Lukyanenko V, et al. Underlying mechanisms of symmetric calcium wave propagation in rat ventricular myocytes. *Biophys J* 2001; 80: 1-11.

[32] Engel J, Fechner M, Sowerby AJ, et al. Anisotropic propagation of Ca^{2+} waves in isolated cardiomyocytes. *Biophys J* 1994; 66: 1756-1762.

[33] Arif S, Lai C-H, Nadarajah R. Modelling stochastic calcium waves in cardiac myocytes based on the two-pool CICR model. *Computing in Cardiology* 2017b; Volume 44. doi:10.22489/CinC.2017.315-092 (In Press)

[34] Driscoll TA, Vavasis SA. Numerical conformal mapping using cross-ratios and Delaunay triangulation. *SIAM J Sci Comput* 1998; 19: 1783-1803.

[35] Takamatsu T, Wier WG. Calcium waves in mammalian heart: quantification of origin, magnitude, waveform, and velocity. *FASEB Journal* 1990; 4: 1519-1525.

[36] Dupont G, Goldbeter A. Oscillations and waves of cytosolic calcium: insights from theoretical models. *BioEssays* 1992; 14: 485-493.

[37] Cheng H, Lederer WJ. Calcium sparks. *Physiol Rev* 2008; 88: 1491-1545.

[38] Fearnley CJ, Roderick HL, Bootman MD. Calcium signalling in cardiac myocytes. *Cold Spring Harb Perspect Biol* 2011.

[39] Bers DM, Shannon TR. Calcium movements inside the sarcoplasmic reticulum of cardiac myocytes. *J Mol Cell Cardiol* 2013; 58: 59-66.